# High-order numerical simulation of fluid-structure interaction in the human larynx

Martin Larsson

ONERA-DAFE,
8 rue des Vertugadins,
F-92190 Meudon, France
E-mail: martin.larsson@onera.fr

Bernhard Müller*

Department of Energy and Process Engineering,
Norwegian University of Science and Technology (NTNU),
Kolbjørn Hejes vei 2, NO-7491 Trondheim, Norway
Fax: +47 73593491
E-mail: bernhard.muller@ntnu.no
*Corresponding author

**Abstract:** We present a 2D model of the human larynx able to reproduce the self-sustained oscillating interaction between the airflow and the vocal folds. We describe the interaction of the compressible flow and the elastic structure in an ALE formulation. Our solver uses globally fourth-order accurate Summation By Parts (SBP) finite difference operators in space and a fourth-order explicit method in time. We derive Simultaneous Approximation Term (SAT) expressions that impose the velocity and traction boundary conditions weakly. We present results from simulations with realistic parameters for human phonation.

**Keywords:** fluid-structure interaction; high-order finite difference method; phonation.

**Reference** to this paper should be made as follows: Larsson, M. and Müller, B. (2012) 'High-order numerical simulation of fluid-structure interaction in the human larynx', *Progress in Computational Fluid Dynamics*, Vol. 12, Nos. 2/3, pp.164–175.

**Biographical notes:** M. Larsson did his MSc in Engineering Physics at Uppsala University, Sweden, in 2007. He received his PhD in 2010 under the supervision of B. Müller from the Norwegian University of Science and Technology (NTNU) at Trondheim, Norway. He is presently working on a postdoc position at ONERA in Meudon, France, investigating aerodynamic stability for low-aspect ratio flapping wings. His research interests include fluid-structure interaction, phonation and numerical and aerodynamic stability.

B. Müller did his Diploma in Mathematics at the University of Cologne, Germany, in 1978. In 1981, he obtained the VKI-Diploma in Aeronautics-Aerospace from the von Karman Institute for Fluid Dynamics, Belgium. He received his PhD in 1985 from the Faculty of Mechanical Engineering, RWTH Aachen University, Germany. During 1985–1987, he was a postdoc at FFA, The Aeronautical Research Institute of Sweden. He served as a Research Scientist at the Institute for Theoretical Fluid Mechanics of DLR in Göttingen 1987–1990. During 1990–1996, he was appointed as an Assistant Professor at the Institute of Fluid Dynamics of ETH Zurich, Switzerland, where he did his habilitation in theoretical fluid mechanics in 1997. After stays at the Faculty of Applied Mathematics, University of Twente, The Netherlands, 1996–1997, and at the Department of Mathematics of Luleå University of Technology, Sweden, 1997–1998, he joined Uppsala University, Sweden, as an Associate Professor at the Department of Information Technology 1998–2007. Since 2007, he has been a Professor of Computational Fluid Dynamics (CFD) at the Department of Energy and Process Engineering of the Norwegian University of Science and Technology (NTNU). His research interests include CFD, computational aeroacoustics, fluid-structure interaction, bio-fluid dynamics and multiphase flow simulation.

## 1 Introduction

Our voice is generated in our larynx by the vibrating vocal folds interacting with the airstream from the lungs. The vocal folds, or vocal cords, are two symmetric membranes that protrude from the walls of the larynx at the top of the trachea of humans and most mammals forming a slit-like opening known as the glottis in the airway. In a simplified three-layer model, the vocal folds are composed of the thyroarytenoid muscle, also known as the vocal fold muscle, and the vocal ligament covered by a mucous layer, cf. Figure 1. During normal breathing, the vocal tract is open and air can pass unobstructedly. During phonation, the vocal fold muscle is tensed in the longitudinal direction so that the glottal opening becomes narrower. As the high-pressure air expelled from the lungs is forced through this narrow opening, it pushes the vocal folds apart. The air column gains momentum, and the velocity in the glottis increases. The increase in velocity causes a pressure drop in the glottis according to the Bernoulli principle. The decrease in pressure leads to an aerodynamic force, which together with the elastic force in the vocal folds strives to close the glottis. A build-up in pressure upstream of the glottis resulting from the closure leads to a pressure force, which opens the vocal folds and allows the passage of air. Under favourable circumstances, this process is repeated in a self-sustained manner and driven only by the pressure from the lungs. It is important to point out that no periodic contraction of muscles occurs during phonation. The opening and closing of the glottis is in this respect a passive process (Titze, 2000).

**Figure 1** Schematic view of the human larynx (see online version for colours)

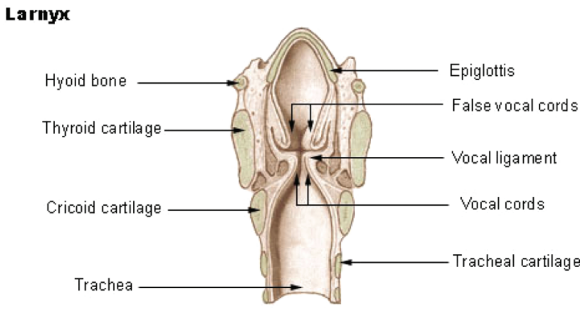


During normal speech, the vocal folds collide with each other, closing the glottis completely. However, in certain types of phonation such as a very breathy voice or while whispering or hissing, the vocal folds do not necessarily make contact. The outermost mucous layer of the vocal folds have been shown to play an important role in the self-sustained oscillation, facilitating the vibrations of the much stiffer ligament (Titze, 2000).

As the vocal folds oscillate rapidly, they generate a fundamental frequency. When we speak normally, only the lowest mode of vibration is excited, in which all the layers of the vocal folds vibrate symmetrically and as a whole. Higher modes of oscillation can, however, be excited to produce higher pitched tones for example when singing. By stretching the vocal fold muscle, the vocal fold length changes as well as the stiffness, and higher modes can thus be created. These higher modes correspond to an oscillation concentrated mainly to the ligament or the mucous layer and have a higher frequency. The different modes of oscillation are commonly referred to as registers (modal, falsetto, etc.) and singers are often particularly good at smoothing out the transition between these registers (Titze, 2008).

The acoustic signal resulting from the glottal flow interacting with the vibrating vocal folds is further modified by the vocal tract, which functions as an acoustic filter. By changing the shape of the vocal tract, different frequencies are amplified and suppressed so that a multitude of different vowels can be formed from the same source signal.

The airflow and vocal folds in the larynx are intrinsically 3D and would need to be modelled as such to obtain a reliable flow field downstream of the glottis. However, the shapes exhibited by the glottis at different time instants during the vibratory cycle show little variation in the transverse direction of the vocal fold. Especially in configurations when the glottis is almost closed, the slit-like opening formed by the two vocal folds can be considered as two-dimensional. In configurations where the glottis is fully open, transverse effects may be important and a 2D model might not be able to accurately represent the flow field during those parts of the cycle. However, since most of the vortex dynamics takes place during the almost closed phases, the acoustic pressure variations emitted by those vortices can be approximately represented in a 2D geometry.

The computational models for self-sustained vibrations of vocal folds have advanced from simple models based on the Bernoulli equation for the airflow and mass-spring models for the vocal folds used in the 1970s to full-fledged 2D and 3D unsteady Fluid-Structure Interactions (FSIs) coupling the Navier–Stokes equations and Navier's equation (Titze, 2000; Luo et al., 2008; Link et al., 2009). In general, lower-order finite difference, volume and element methods have been used.

In this paper, we employ a high-order finite difference approach based on SBP operators (Strand, 1994; Gustafsson et al., 1995; Gustafsson, 2008) to solve the compressible Navier–Stokes equations and the linear elastic wave equation, i.e., Navier's equation. Fluid and structure interact in a two-way coupling, meaning that fluid stresses deform the flexible structure, which in turn causes the fluid to conform to the new structural boundary via no-slip boundary conditions. The traction boundary conditions and the location and velocity of the vocal fold boundaries are communicated between structure and fluid at the beginning of each time step of the explicit Runge-Kutta time stepping of fluid and structure. While the velocity and traction boundary conditions for the structure are weakly imposed using the SAT approach (Larsson and Müller, 2011), the no-slip boundary conditions for the fluid are enforced

by injecting the data supplied by the structure. The approach has been tested for a 2D model of the larynx and the vocal folds.

Like the other methods for FSI in the human larynx cited earlier, the present method cannot handle contact of the vocal folds occurring during their collision, because it cannot handle cells with zero volume. We therefore consider a case where the vocal folds do not collide. As mentioned earlier, such situations occur in nature for breathy voices and when whispering or hissing sounds are produced. To model typical human phonation, a contact model and a special treatment for the closing glottis would be needed.

The present work is based on Martin Larsson's PhD thesis (Larsson, 2010) and the six papers by Larsson and Müller (2009a, 2009b, 2011, 2010a, 2010b) contained therein.

## 2 Governing equations

### 2.1 Compressible Navier–Stokes equations

The perturbation formulation is used to minimise cancellation errors when discretising the Navier–Stokes equations for compressible low Mach number flow (Sesterhenn et al., 1999; Müller, 1996). The 2D compressible Navier–Stokes equations in conservative form can be expressed in perturbation form as Müller (2008) and Larsson and Müller (2009a)

$$U'_t + F^{c\prime}_x + G^{c\prime}_y = F^{v\prime}_x + G^{v\prime}_y, \tag{1}$$

where the vector $U'$ denotes the perturbation of the conservative variables with respect to the stagnation values. $U'$ and the inviscid (superscript $c$) and viscous (superscript $v$) flux vectors can be found in, e.g., Larsson and Müller (2009a).

General moving geometries are treated by a time-dependent coordinate transformation $\tau = t$, $\xi = \xi(t,x,y)$, $\eta = \eta(t,x,y)$. The transformed 2D conservative compressible Navier–Stokes equations in perturbation form read (Larsson and Müller, 2009a)

$$\widehat{U}'_\tau + \widehat{F}'_\xi + \widehat{G}'_\eta = 0, \tag{2}$$

where $\widehat{U}' = J^{-1}U'$, $\widehat{F}' = J^{-1}(\xi_t U' + \xi_x(F^{c\prime} - F^{v\prime}) + \xi_y(G^{c\prime} - G^{v\prime}))$ and $\widehat{G}' = J^{-1}(\eta_t U' + \eta_x(F^{c\prime} - F^{v\prime}) + \eta_y(G^{c\prime} - G^{v\prime}))$. Equation (2) constitutes the ALE formulation of the 2D compressible Navier–Stokes equations in perturbation form.

No-slip adiabatic wall boundary conditions are used at the upper and lower walls of the vocal tract including the moving boundaries of the upper and lower vocal folds, cf. Figure 2. The Navier–Stokes Characteristic Boundary Conditions (NSCBC) technique by Poinsot and Lele (1992) is employed at the outflow, i.e., the right boundary in Figure 2 (Larsson and Müller, 2009b). At the inflow, i.e., the left boundary in Figure 2, the pressure, temperature and $y$-component of velocity are imposed as $p = p_{\text{atm}} + \Delta p, T = T_0 = 310\,\text{K}$, and $v = 0$, respectively. The $x$-component of velocity $u$ at the inflow and the pressure $p$ at the walls are computed from the 2D compressible Navier–Stokes Equations (2) discretised at the boundaries.

**Figure 2** Computational fluid and structure domains of airflow and vocal folds, respectively (see online version for colours)

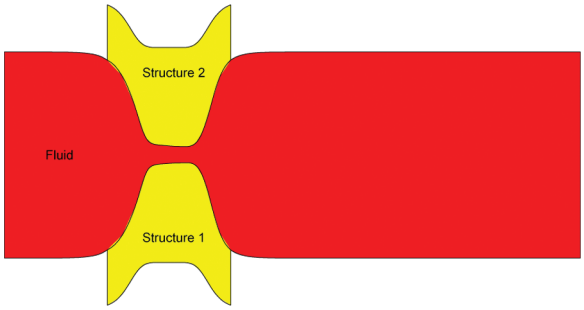


### 2.2 Linear elastic wave equation

The 2D linear elastic wave equation written as a first-order hyperbolic system reads in Cartesian coordinates

$$q_t = Aq_x + Bq_y, \tag{3}$$

where the unknown vector $q = (u, v, f, g, h)^T$ contains the velocity components $u, v$ and the stress components $f, g, h$. The coefficient matrices $A$ and $B$ depend on the the Lamé parameters $\lambda, \mu$ and the density $\rho$, which are here all taken to be constant in space and time, cf. e.g., Fornberg (1998) and LeVeque (2002).

The linear combination $P(k_x, k_y) = k_x A + k_y B$ can be diagonalised with real eigenvalues and linearly independent eigenvectors. The eigenvalue matrix is defined as the diagonal matrix with the eigenvalues of $P(k_x, k_y)$ in decreasing order,

$$\begin{aligned}\tilde{\Lambda}(k_x, k_y) &= (k_x^2 + k_y^2)^{1/2}\text{diag}(c_p, c_s, 0, -c_s, -c_p) \\ &= \text{diag}\left\{\tilde{\lambda}_i(k_x, k_y)\right\}_{i=1}^{5},\end{aligned} \tag{4}$$

where the wave speeds are $c_p = \sqrt{(\lambda + 2\mu)/\rho}$ and $c_s = \sqrt{\mu/\rho}$, referred to as primary (or pressure) and secondary (or shear) wave speeds, respectively.

To treat curvilinear grids, we introduce the mapping $x = x(\xi, \eta)$, $y = y(\xi, \eta)$. The Jacobian determinant $J^{-1}$ of the transformation is given by $J^{-1} = x_\xi y_\eta - x_\eta y_\xi$ and the linear elastic wave equation can then be written as

$$\hat{q}_t = (\hat{A}\hat{q})_\xi + (\hat{B}\hat{q})_\eta \tag{5}$$

where the hats signify that the quantities are in transformed coordinates, i.e., $\hat{q} = J^{-1}q$, $\hat{A} = \xi_x A + \xi_y B$ and $\hat{B} = \eta_x A + \eta_y B$.

### 2.3 Characteristic variables

To describe the SAT expressions in transformed coordinates we need to find the characteristic variables for the transformed equation in which the coefficient matrices are linear combinations of the coefficient matrices in the $x$- and $y$-directions.

$$\hat{q}_t = ((k_x A + k_y B)\hat{q})_k \tag{6}$$

for $k = \xi, \eta$. We form the linear combination $P(k_x, k_y) = k_x A + k_y B$. The coefficient matrices $A$ and $B$ have the same set of eigenvalues $\Lambda = \mathrm{diag}(c_p, c_s, 0, -c_s, -c_p)$, whereas for the linear combination $P(k_x, k_y)$ we get $\tilde{\Lambda}(k_x, k_y) = (k_x^2 + k_y^2)^{1/2}\Lambda$. To find the linearly independent eigenvectors of $P(k_x, k_y)$, we solve the under-determined system $(P(k_x, k_y) - \tilde{\lambda}_i I)v_i = 0$ for $i = 1, \ldots, 5$. These five eigenvectors $v_i$ become the columns in the eigenvector matrix $T(k_x, k_y)$, cf. Appendix A. We have some degrees of freedom in choosing $T$, because each column can be scaled by any non-zero constant. The inverse of this matrix is obtained with a symbolic computer program, cf. Appendix A where we have introduced the following abbreviations $\bar{k} = (k_x^2 - k_y^2)/(k_x^2 + k_y^2)$, $r = (k_x^2 + k_y^2)^{1/2}$, $\tilde{c}_p = rc_p$, $\tilde{c}_s = rc_s$, $\alpha = (\lambda + 2\mu)/\lambda$ and $\beta = \alpha\lambda/\mu$. For all directions $(k_x, k_y)$ we have that $T^{-1}(k_x, k_y)P(k_x, k_y)T(k_x, k_y) = \tilde{\Lambda}(k_x, k_y)$. The transformation to characteristic variables $u$ is given by $u^{(k)} = T^{-1}(k_x, k_y)\hat{q}$ for each of the two coordinate directions $k = \xi, \eta$. The transformation back to flow variables is given by $\hat{q} = T(k_x, k_y)u^{(k)}$.

## 3 Time stable high order difference method

### 3.1 Energy method

The energy method is a general technique to prove sufficient conditions for well posedness of Partial Differential Equations (PDEs) and stability of difference methods with general boundary conditions.

Consider the solution of the model problem in 1D with

$$\begin{aligned} u_t &= \lambda u_x, \quad \lambda > 0,\ 0 \le x \le 1,\ t \ge 0, \\ u(x,0) &= f(x), \quad u(1,t) = g(t). \end{aligned} \tag{7}$$

Here, the symbol $\lambda$ represents a general eigenvalue for the hyperbolic system and should not be confused with the Lamé parameter. Define the $L_2$ scalar product for real functions $v$ and $w$ on the interval $0 \le x \le 1$ as

$$(v, w) = \int_0^1 v(x)w(x)dx \tag{8}$$

which defines a norm of the continuous solution at some time $t$ and an energy $E(t) = \|u(\cdot, t)\|^2 = (u, u)$. Using integration by parts $(v, w_x) = v(1,t)w(1,t) - v(0,t)w(0,t) - (v_x, w)$, we get $\frac{dE}{dt} = \frac{d\|u\|^2}{dt} = (u_t, u) + (u, u_t) = \lambda[(u_x, u) + (u, u_x)] = \lambda[(u_x, u) + [u^2]_0^1 - (u_x, u)] = \lambda[u^2(1,t) - u^2(0,t)]$. If $\lambda > 0$, the boundary condition $u(1,t) = 0$ yields a non-growing solution (note that periodic boundary conditions would also yield a non-growing solution), i.e., $E(t) \le E(0) = \|f(x)\|^2$. Thus, the energy of the solution is bounded by the energy of the initial data. As a unique solution of the Initial-Boundary Value Problem (IBVP) (7) exists, the problem is well posed.

### 3.2 Summation by parts operators

The idea behind the SBP technique for first-order IBVP is to devise difference approximations $Q$ of the first spatial derivative satisfying the discrete analogue of integration by parts called the SBP property (Gustafsson, 2008). To outline the idea for the numerical solution of (7), we introduce the equidistant grid $x_j = jh$, $j = 0, \ldots, N$, $h = 1/N$, and a solution vector containing the solution at the discrete grid points, $\mathbf{u} = (u_0(t), u_1(t), \ldots, u_N(t))^T$. The semi-discrete problem can be stated using a difference operator $Q$ approximating the first derivative in space,

$$\frac{d\mathbf{u}}{dt} = \lambda Q\mathbf{u}, \quad u_j(0) = f(x_j). \tag{9}$$

We also define a discrete scalar product and corresponding norm and energy by

$$\begin{aligned} (\mathbf{u}, \mathbf{v})_h &= h\sum_{i,j} h_{ij}u_i v_j = h\mathbf{u}^{\mathrm{T}}H\mathbf{v}, \\ E_h(t) &= \|\mathbf{u}\|_h^2 = (\mathbf{u}, \mathbf{u})_h, \end{aligned} \tag{10}$$

where the symmetric and positive definite norm matrix $H = \mathrm{diag}(H_L, I, H_R)$ has components $h_{ij}$. In order for Equation (10) to define a scalar product, $H_L$ and $H_R$ must be symmetric and positive definite. We say that the difference operator $Q$ satisfies the SBP property, if

$$(\mathbf{u}, Q\mathbf{v})_h = u_N v_N - u_0 v_0 - (Q\mathbf{u}, \mathbf{v})_h. \tag{11}$$

It can be seen that this property is satisfied, if the matrix $G = HQ$ satisfies the condition that $G + G^{\mathrm{T}} = \mathrm{diag}(-1, 0, \ldots, 0, 1)$. If $Q$ satisfies the SBP property (11), then the energy method for the discrete problem yields:

$$\begin{aligned} \frac{dE_h}{dt} = \frac{d\|\mathbf{u}\|_h^2}{dt} &= (\mathbf{u}_t, \mathbf{u})_h + (\mathbf{u}, \mathbf{u}_t)_h \\ &= \lambda[(Q\mathbf{u}, \mathbf{u})_h + (\mathbf{u}, Q\mathbf{u})_h] \\ &= \lambda[(Q\mathbf{u}, \mathbf{u})_h + u_N^2 - u_0^2 - (Q\mathbf{u}, \mathbf{u})_h] \\ &= \lambda[u_N^2 - u_0^2]. \end{aligned} \tag{12}$$

How to obtain time stability $dE_h/dt \le 0$, i.e., no energy growth in time, is the topic of the next section.

For diagonal $H_L$ and $H_R$, there exist difference operators $Q$ accurate to order $\mathcal{O}(h^{2s})$ in the interior and $\mathcal{O}(h^s)$ near the boundaries for $s = 1, 2, 3$ and 4. These operators have an effective order of accuracy $\mathcal{O}(h^{s+1})$ in the entire domain. Explicit forms of such operators $Q$ and norm matrices $H$ were derived by Strand (1994).

For this study, we use an SBP operator based on the central sixth-order explicit finite difference operator

$(s = 3)$, which has been modified near the boundaries to satisfy the SBP property giving an effective $\mathcal{O}(h^4)$ order of accuracy in the whole domain (Strand, 1994).

### 3.3 Simultaneous approximation term

Since the term $\lambda u_N^2$ in Equation (12) is non-negative, time stability does not follow when using the injection method for the SBP operator, i.e., by using $u_N(t) = g(t)$, since injection affects the operator $Q$ and the SBP property (11) (Strand, 1994; Gustafsson, 2008). In contrast, the SAT method by Carpenter et al. (1994) is an approach where a linear combination of the boundary condition and the differential equation is solved at the boundary. This leads to a weak imposition of the physical boundary condition. The imposition of SAT boundary conditions is accomplished by adding a source term to the difference operator, proportional to the difference between the value of the discrete solution $u_N$ and the boundary condition. The SAT method for the semidiscrete advection Equation (9) can be expressed as

$$\frac{d\mathbf{u}}{dt} = \lambda Q\mathbf{u} - \lambda\tau\mathbf{S}(u_N - g(t))$$

where $\mathbf{S} = h^{-1}H^{-1}(0, 0, \ldots, 0, 1)^{\mathrm{T}}$ and $\tau$ is a free parameter.

The added term does not alter the accuracy of the scheme, since it vanishes when the analytical solution is substituted. Thus, we can imagine the SAT expression as a modification to the difference operator so that we are effectively solving an equation $\mathbf{u}_t = \lambda\widetilde{Q}\mathbf{u}$ with $\widetilde{Q} = Q + Q^{\mathrm{sat}}$ where the boundary conditions are accounted for by the operator itself. When $H$ is diagonal, the scheme is only modified at one point, namely at the point where the boundary condition is imposed. We can now show that this scheme is time stable for $g(t) = 0$. The energy rate for the solution of the semi-discrete equation is $\frac{dE_h}{dt} = \frac{d\|\mathbf{u}\|_h^2}{dt} = (\mathbf{u}_t, \mathbf{u})_h + (\mathbf{u}, \mathbf{u}_t)_h = \lambda[(Q\mathbf{u} - \tau\mathbf{S}u_N, \mathbf{u})_h + (\mathbf{u}, Q\mathbf{u} - \tau\mathbf{S}u_N)_h] = \lambda[(Q\mathbf{u}, \mathbf{u})_h - \tau(\mathbf{S}, \mathbf{u})_h u_N + (\mathbf{u}, Q\mathbf{u})_h - \tau(\mathbf{u}, \mathbf{S})_h u_N] = \lambda[(1 - 2\tau)u_N^2 - u_0^2]$ since $(\mathbf{S}, \mathbf{u})_h = (\mathbf{u}, \mathbf{S})_h = h\mathbf{u}^{\mathrm{T}}Hh^{-1}H^{-1}(0, 0, \ldots, 0, 1)^{\mathrm{T}} = u_N$. The discretisation is time stable if $\tau \geq 1/2$.

The extension of the time stable SAT method to 1D hyperbolic systems

$$u_t = \Lambda u_x \tag{13}$$

with a diagonal $r \times r$ coefficient matrix $\Lambda$ is performed in the following way (Carpenter et al., 1994). The coefficient matrix $\Lambda$ is chosen such that the diagonal entries appear in descending order, i.e., $\lambda_1 > \lambda_2 > \cdots > \lambda_k > 0 > \lambda_{k+1} > \cdots > \lambda_r$. The solution vector $u$ is split into two parts corresponding to positive and negative diagonal elements $u^{\mathrm{I}} = (u^{(1)}, \ldots, u^{(k)})^T$ and $u^{\mathrm{II}} = (u^{(k+1)}, \ldots, u^{(r)})^T$, where $u^{(i)}$ is the $i$th component of $u$. Since the $i$th component of (13) reads $u_t^{(i)} = \lambda_i u_x^{(i)}$, the vectors $u^{\mathrm{I}}$ and $u^{\mathrm{II}}$ are transported to the left and right, respectively. Therefore, boundary conditions have to be prescribed on $u^{\mathrm{I}}$ at the right boundary $x = 1$ and on $u^{\mathrm{II}}$ at the left boundary $x = 0$. To allow for coupling of the in- and outgoing variables at the boundaries, we introduce a $k \times (r - k)$ matrix $R$ and a $(r - k) \times k$ matrix $L$. We define boundary functions $g^{\mathrm{I}}(t) = (g^{(1)}(t), \ldots, g^{(k)}(t))$ and $g^{\mathrm{II}}(t) = (g^{(k+1)}(t), \ldots, g^{(r)}(t))$. Then, the boundary conditions are given by

$$\begin{aligned} u^{\mathrm{I}}(1, t) &= Ru^{\mathrm{II}}(1, t) + g^{\mathrm{I}}(t), \\ u^{\mathrm{II}}(0, t) &= Lu^{\mathrm{I}}(0, t) + g^{\mathrm{II}}(t). \end{aligned} \tag{14}$$

Under the constraint $|R\|L| \leq 1$, the IBVP (13) with (14) is well posed (Carpenter et al., 1994), where the matrix 2-norm is defined by $|R| = \sqrt{\rho(R^T R)}$ and $\rho(A)$ is the spectral radius of $A$.

We define the grid functions of the components of $u$ as $\mathbf{u}^{(i)} = (u_0^{(i)}, \ldots, u_N^{(i)})^T$, where $u_j^{(i)} = u^{(i)}(x_j)$. Then, we define the grid functions of $u^{\mathrm{I}}$ and $u^{\mathrm{II}}$ as $\mathbf{u}^{\mathrm{I}} = (\mathbf{u}^{(1)}, \ldots, \mathbf{u}^{(k)})$ and $\mathbf{u}^{\mathrm{II}} = (\mathbf{u}^{(k+1)}, \ldots, \mathbf{u}^{(r)})$. The boundary conditions (14) for the semi-discretisation of (13) are imposed by the SAT method as Carpenter et al. (1994)

$$\begin{aligned} \tfrac{d\mathbf{u}^{(i)}}{dt} = {} & \lambda_i Q\mathbf{u}^{(i)} - \lambda_i\tau\mathbf{S}^{(i)}(u_N^{(i)} - \\ & (R\mathbf{u}_N^{\mathrm{II}})^{(i)} - g^{(i)}(t)), \quad 1 \leq i \leq k \\ \tfrac{d\mathbf{u}^{(i)}}{dt} = {} & \lambda_i Q\mathbf{u}^{(i)} + \lambda_i\tau\mathbf{S}^{(i)}(u_0^{(i)} - \\ & (L\mathbf{u}_0^{\mathrm{I}})^{(i-k)} - g^{(i)}(t)), \quad k + 1 \leq i \leq r \end{aligned} \tag{15}$$

where $\mathbf{S}^{(i)} = h^{-1}H^{-1}(0, 0, \ldots, 1)^{\mathrm{T}}$ for $1 \leq i \leq k$ and $\mathbf{S}^{(i)} = h^{-1}H^{-1}(1, 0, \ldots, 0)^{\mathrm{T}}$ for $k + 1 \leq i \leq r$. Regarding the notation, $(R\mathbf{u}_N^{\mathrm{II}})^{(i)}$ should be interpreted as follows: $\mathbf{u}_N^{\mathrm{II}} = (u_N^{(r-k)}, \ldots, u_N^{(r)})^T$ is the last row of $u^{\mathrm{II}}$ transposed. Multiplying $R$ by $\mathbf{u}_N^{\mathrm{II}}$ yields a new vector of which the $(i)$th component is taken. The interpretation of $\mathbf{u}_0^{\mathrm{I}}$ is similar with $\mathbf{u}_0^{\mathrm{I}} = (u_0^{(1)}, \ldots, u_0^{(k)})^T$. As shown by Carpenter et al. (1994), the SAT method is both stable in the classical sense and time stable provided that

$$\frac{1 - \sqrt{1 - |R\|L|}}{|R\|L|} \leq \tau \leq \frac{1 + \sqrt{1 - |R\|L|}}{|R\|L|}. \tag{16}$$

## 4 Sat expressions for the linear elastic wave equation

### Notation for boundary conditions

We adopt the notation $u(k_0, t) = \bar{u}(k = k_0, t)$ to represent a 1D boundary condition on the solution variable $u$ in any direction $k$ where $k = \xi$ or $k = \eta$ and $\bar{u}(k, t)$ is the given functions of time on the boundaries $k_0 = 0$ and $k_0 = 1$, which the solution variable $u$ should match on those boundaries. For example, $\bar{u}(\xi = 1, t)$ is the given $u$-velocity at the boundary $\xi = 1$ and $u(1, t)$ is the corresponding solution to the equations. In 2D, the boundary condition also depends on the second coordinate direction, which we indicate by $\bar{u}(\xi = 1, \eta, t)$ and $\bar{u}(\xi, \eta = 1, t)$ for boundary conditions in the $\xi$- and

$\eta$-directions, respectively. Finally, for the discretised 2D boundary conditions, we write instead $\bar{u}_j(\xi = 1, t) = \bar{u}(\xi = 1, \eta_j, t)$ and $\bar{u}_i(\eta = 1, t) = \bar{u}(\xi_i, \eta = 1, t)$.

### *4.1 Presentation of SAT expressions*

The SAT expressions for the linear elastic wave equation are summarised here.

To apply the theory for 1D linear diagonalised hyperbolic systems (13), we have to express (6) in characteristic form, i.e., $u_t = \tilde{\Lambda} u_k$. $u = u^{(k)} = T^{-1}(k_x, k_y)\hat{q}$ is the vector of the characteristic variables in the $k$-direction where $\hat{q} = J^{-1}(u, v, f, g, h)^T$. $\tilde{\Lambda} = \tilde{\Lambda}(k_x, k_y)$ is the diagonal matrix with the eigenvalues of $P(k_x, k_y)$ where $k = \xi$ or $k = \eta$, and $u_k = \frac{\partial u}{\partial k}$.

We form the two sub-vectors corresponding to positive and negative eigenvalues as

$$u^{\mathrm{I}}(k_x, k_y) = (u_1, u_2)^T, \quad u^{\mathrm{II}}(k_x, k_y) = (u_4, u_5)^T \tag{17}$$

with the aim to form boundary conditions with the matrices $R$ and $L$. Since the components of $u^{\mathrm{I}}$ and $u^{\mathrm{II}}$ contain velocity and stress components in positive or negative pairs, it is easy to find $2 \times 2$ matrices $L$ and $R$ in Equation (14) to prescribe velocity or traction components as boundary conditions $g^{\mathrm{I}}$ and $g^{\mathrm{II}}$. Let us illustrate this approach for prescribing the velocity components $u$ and $v$ at the boundaries.

Looking at the characteristic variables, we find the following identities to prescribe the velocity components $u_n = (k_x u + k_y v)/r$ and $u_t = (-k_y u + k_x v)/r$ normal and tangential, respectively, to a grid line $k = const$:

$$u^{\mathrm{I}}(k_x, k_y) - \begin{bmatrix} 0 & 1 \\ -1 & 0 \end{bmatrix} u^{\mathrm{II}}(k_x, k_y) = \frac{J^{-1}}{r} \begin{bmatrix} \frac{\lambda}{\tilde{c}_p} u_n \\ u_t \end{bmatrix} \tag{18}$$

$$u^{\mathrm{II}}(k_x, k_y) - \begin{bmatrix} 0 & -1 \\ 1 & 0 \end{bmatrix} u^{\mathrm{I}}(k_x, k_y) = \frac{J^{-1}}{r} \begin{bmatrix} u_t \\ -\frac{\lambda}{\tilde{c}_p} u_n \end{bmatrix} \tag{19}$$

Thus, using the matrices $L = \begin{bmatrix} 0 & -1 \\ 1 & 0 \end{bmatrix}$ and $R = \begin{bmatrix} 0 & 1 \\ -1 & 0 \end{bmatrix}$ in Equation (14), we can prescribe boundary conditions for $g^{\mathrm{I}}(k_x, k_y, t) = \frac{J^{-1}}{r^2} \begin{bmatrix} \frac{\lambda}{\tilde{c}_p}(k_x u + k_y v) \\ -k_y u + k_x v \end{bmatrix}$ and $g^{\mathrm{II}}(k_x, k_y, t) = \frac{J^{-1}}{r^2} \begin{bmatrix} -k_y u + k_x v \\ -\frac{\lambda}{\tilde{c}_p}(k_x u + k_y v) \end{bmatrix}$, cf. (20) and (21) below. Note that $L$ and $R$ are independent of the direction, but depend on the particular type of boundary condition to be imposed (velocity or traction). For boundary conditions on the velocities $u$ and $v$, we get using the identities (18)–(19) the following expressions

$$\begin{aligned} R &= \begin{bmatrix} 0 & 1 \\ -1 & 0 \end{bmatrix}, \quad g^{\mathrm{I}}(k_x, k_y, t) \\ &= \frac{J^{-1}}{r^2} \begin{bmatrix} \frac{\lambda}{\tilde{c}_p}(k_x \bar{u}(k=1,t) + k_y \bar{v}(k=1,t)) \\ -k_y \bar{u}(k=1,t) + k_x \bar{v}(k=1,t) \end{bmatrix}, \\ L &= \begin{bmatrix} 0 & -1 \\ 1 & 0 \end{bmatrix}, \quad g^{\mathrm{II}}(k_x, k_y, t) \\ &= \frac{J^{-1}}{r^2} \begin{bmatrix} -k_y \bar{u}(k=0,t) + k_x \bar{v}(k=0,t) \\ -\frac{\lambda}{\tilde{c}_p}(k_x \bar{u}(k=0,t) + k_y \bar{v}(k=0,t)) \end{bmatrix}, \end{aligned} \tag{20, 21}$$

where $\bar{u}(k,t), \bar{v}(k,t)$ are the given boundary conditions on $u, v$ at the boundaries.

The boundary conditions on the stresses come from a traction boundary condition of the form $\sigma \mathbf{n} = \bar{\mathbf{t}}$ where $\bar{\mathbf{t}} = (\bar{t}_x, \bar{t}_y)^T$ is the given traction vector from the fluid and $\sigma = \begin{bmatrix} f & g \\ g & h \end{bmatrix}$ is the Cauchy stress tensor in the structure. The unit normal $\mathbf{n}$ can be expressed in terms of the coordinate transformation as $\mathbf{n} = (1/r)(k_x, k_y)^T$, cf. Figure 3, and the components of $g^{\mathrm{I}}$ and $g^{\mathrm{II}}$ for traction boundary conditions can be written as

$$\begin{aligned} R &= \begin{bmatrix} 0 & -1 \\ 1 & 0 \end{bmatrix}, \quad g^{\mathrm{I}}(k_x, k_y, t) = \frac{J^{-1}}{r^2} \\ &\quad \times \begin{bmatrix} \frac{1}{\alpha r}(k_x \bar{t}_x(k=1,t) + k_y \bar{t}_y(k=1,t)) \\ \frac{r}{\rho \tilde{c}_s}(-k_y \bar{t}_x(k=1,t) + k_x \bar{t}_y(k=1,t)) \end{bmatrix}, \\ L &= \begin{bmatrix} 0 & 1 \\ -1 & 0 \end{bmatrix}, \quad g^{\mathrm{II}}(k_x, k_y, t) = \frac{J^{-1}}{r^2} \\ &\quad \times \begin{bmatrix} \frac{r}{\rho \tilde{c}_s}(k_y \bar{t}_x(k=0,t) - k_x \bar{t}_y(k=0,t)) \\ \frac{1}{\alpha r}(k_x \bar{t}_x(k=0,t) + k_y \bar{t}_y(k=0,t)) \end{bmatrix}. \end{aligned} \tag{22, 23}$$

Therefore, it is sufficient to specify the two parameters $\bar{t}_x$ and $\bar{t}_y$ on each boundary instead of all of the three $\bar{f}, \bar{g}, \bar{h}$, which might otherwise violate well posedness.

**Figure 3** Coordinate transformation

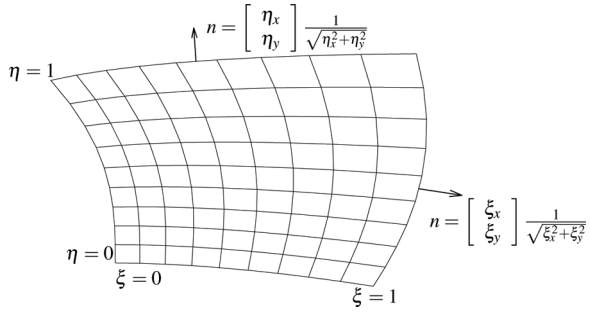


Inserting the definitions of $g^{\mathrm{I,II}}$ and $R, L$ gives with Equation (15) a SAT expression (which we simply call SAT) for each of the five equations in characteristic variables. At a general index $i \in \{0, 1, \ldots, N\}$ in the $k$-direction, the SAT vector for prescribed velocity components will be $SAT_i^{(k)}(k_x, k_y, t) = -\frac{\tau J^{-1}}{h_k r^2}$

$$\begin{bmatrix} \lambda h_{NN}^{-1} \delta_{iN}[k_x(u_N - \bar{u}(k=1,t)) + k_y(v_N - \bar{v}(k=1,t))] \\ \tilde{c}_s \bar{k} h_{NN}^{-1} \delta_{iN}[-k_y(u_N - \bar{u}(k=1,t)) + k_x(v_N - \bar{v}(k=1,t))] \\ 0 \\ \tilde{c}_s \bar{k} h_{00}^{-1} \delta_{i0}[-k_y(u_0 - \bar{u}(k=0,t)) + k_x(v_0 - \bar{v}(k=0,t))] \\ -\lambda h_{00}^{-1} \delta_{i0}[k_x(u_0 - \bar{u}(k=0,t)) + k_y(v_0 - \bar{v}(k=0,t)) \end{bmatrix},$$

where $h_{00}$ and $h_{NN}$ are the first and last entries, respectively, of the diagonal norm matrix $H$. Note that the SAT term for the characteristic variable $u_3$ with

characteristic speed zero is zero, because for $u_3$ no boundary condition must be given. For $k = \xi$, we use the index $i$, while for $k = \eta$ we employ index $j$ for $i$ and $M$ for $N$. Equation (16) implies $\tau = 1$.

For each of the two spatial directions, the transformation matrix $T(k_x, k_y)$ is applied to get the corresponding SAT expressions in flow variables.

$$\overline{\mathrm{SAT}}_i^{(k)} = T(k_x, k_y)\mathrm{SAT}_i^{(k)}(k_x, k_y) \tag{24}$$

for $k = \xi$ and $\eta$. Finally, the total SAT expression is then the sum of the two contributions from the two coordinate directions.

$$\widehat{\overline{\mathrm{SAT}}}_{i,j} = \overline{\mathrm{SAT}}_{i,j}^{(\xi)}(\xi_x, \xi_y) + \overline{\mathrm{SAT}}_{i,j}^{(\eta)}(\eta_x, \eta_y). \tag{25}$$

## 5 Fluid-structure interaction

### 5.1 Arbitrary Lagrangean–Eulerian (ALE) formulation

The displacement of the fluid-structure interface determines the shape of the fluid domain, and the structure velocity at the interface determines the internal grid point velocities in the fluid domain. The left and right boundaries of the fluid domain are the in- and outflow, respectively. The top and bottom parts of the fluid domain are bounded by the flexible vocal folds and the inner wall of the vocal tract, which is here assumed to be rigid. As we do not assume symmetry with respect to the streamwise centreline of the vocal tract, the two vocal folds are solved for individually. In our ALE formulation, the positions and velocities of the grid points in the fluid domain are linearly interpolated along the grid lines connecting the upper and lower vocal folds where the positions and velocities are given by the structure solution. Figure 4 shows the given structure velocities with bold arrows and the interpolated grid point velocities $\dot{x}, \dot{y}$ (thin arrows) for three grid lines.
To obtain the time derivative of $J^{-1}$ as needed in (2), a geometric invariant (Visbal and Gaitonde, 2002) is used. This geometric conservation law states that

$$(J^{-1})_\tau + (J^{-1}\xi_t)_\xi + (J^{-1}\eta_t)_\eta = 0. \tag{26}$$

**Figure 4** The boundary of the fluid domain consists of fixed and flexible parts. The velocity at the boundary of the flexible part determines the internal grid point velocity. Only the lower half of the domain is shown

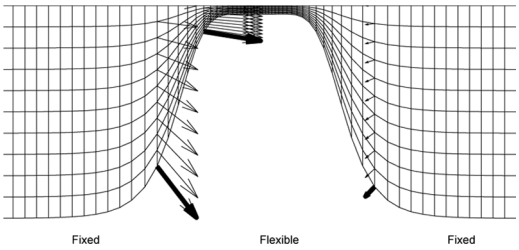


The time derivatives of the computational coordinates $\xi, \eta$ can here be obtained from the grid point velocities $\dot{x}, \dot{y}$ as $\xi_t = -(\dot{x}\xi_x + \dot{y}\xi_y)$, $\eta_t = -(\dot{x}\eta_x + \dot{y}\eta_y)$, which can be seen by differentiating the transformation with respect to $\tau$. With the $\xi$- and $\eta$-derivatives in Equation (26) discretised by the globally fourth-order SBP operator, we get the time derivative $(J^{-1})_\tau$ at each time level. The Jacobian determinant $J^{-1}$ of the coordinate transformation is determined by $J^{-1} = x_\xi y_\eta - x_\eta y_\xi$ and the metric terms by $J^{-1}\xi_x = y_\eta$, $J^{-1}\xi_y = -x_\eta$, $J^{-1}\eta_x = -y_\xi$, $J^{-1}\eta_y = x_\xi$.

### 5.2 Description of fluid-structure interaction algorithm

At the start of a simulation, we construct the fixed reference configuration for the structure and set the initial variables to zero (zero velocity and no internal stresses). The initial conditions for the perturbation variables $U'$ in the fluid domain are taken equal to zero as well (stagnation conditions). In the first time step, the fluid domain is uniquely determined by the reference boundary of the structure. To go from time level $n$ to $n+1$, we first take one time step for the fluid with imposed pressure boundary conditions at the inflow and adiabatic no-slip conditions on the walls, i.e., $\mathbf{u} = \mathbf{u}_w$ and $\partial T/\partial n = 0$. After the fluid time step, the fluid stress on the wall is calculated based on the new fluid velocities and pressures. These fluid stresses $\sigma^f$ are passed on to the structure solver via the traction boundary condition. The force per unit area exerted on a surface element with unit normal $\mathbf{n}$ is $\bar{\mathbf{t}} = \sigma^f \mathbf{n}$, where $\mathbf{n}$ is here the outer unit normal of the structure, calculated from the displacement vector field.

The traction computed at time level $n$ for the fluid is then used to advance the structure solution to time level $n+1$. Note that the traction $\bar{\mathbf{t}}^n$ is used, although $(\sigma^f)^{n+1}\mathbf{n}^n \approx \bar{\mathbf{t}}^{n+1}$ is available. For we employ explicit time integration where we start from time level $n$ for both structure and fluid. The solution for the structure at the new time level gives the velocities and displacements on the boundary, which in turn are used to generate the new fluid grid and internal grid point velocities. This procedure is repeated for each time step.

The fluid-structure interaction algorithm is summarised as follows:

1 Generate the initial fluid grid based on the reference configuration for the structure. $\Rightarrow x^0, \dot{x}^0$.

2 Give initial values for the fluid and the structure. $\Rightarrow F^0, S^0$.

3 For time step $n = 1, 2, \ldots,$ do:

   (a) Calculate the fluid stress on the boundary and calculate the force per unit area, i.e., traction, on the structure via the unit normal. Store the traction vector $\bar{\mathbf{t}}^n$, cf. Figure 5(a).

**Figure 5** Illustration of fluid-structure interaction algorithm: $\Omega^f$, $\Omega^s$: fluid and structure domains. (a) The traction vector $\mathbf{T}(\mathbf{x},t) = \bar{\mathbf{t}}(\mathbf{x},t)$ exerted on the structure by the fluid is calculated on the fluid-structure interface as the fluid stress tensor times the outward unit normal. (b) The grid point velocity $\dot{x}_{i,j}$ at grid point $(i,j)$ is interpolated from the given velocity $\mathbf{v}$ of the structure on the interface

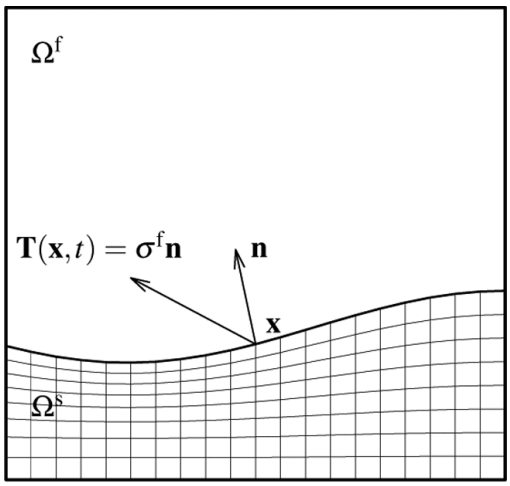


(a)

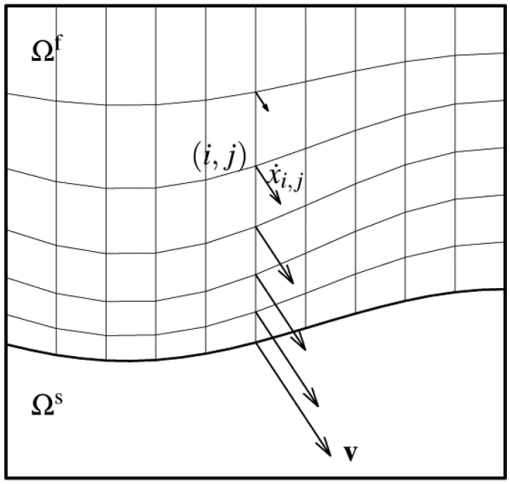


(b)

(b) Take one time step for the fluid: $F^{n+1} = F(x^n, \dot{x}^n)$.

(c) Then the new fluid pressure $p^{n+1}$ and the new fluid velocity $\mathbf{u}^{n+1}$ on the boundary are available.

(d) Take one time step for the structure using the boundary conditions $\bar{\mathbf{t}}^n$: $S^{n+1} = S(\bar{\mathbf{t}}^n)$.

(e) Recalculate the fluid grid and the grid point velocities based on the new structure solution, cf. Figure 5(b). $\Rightarrow x^{n+1}, \dot{x}^{n+1}$.

4 Repeat from 3 with time step $n+1$ until the final time is reached.

## 6 Discretisation

### *Notation*

The Kronecker product of an $n \times m$ matrix $C$ and a $k \times l$ matrix $D$ is the $n \times m$ block matrix

$$C \otimes D = \begin{bmatrix} c_{11}D \cdots c_{1m}D \\ \vdots \quad \ddots \quad \vdots \\ c_{n1}D \cdots c_{nm}D \end{bmatrix}. \tag{27}$$

This notation will be useful for writing the discretisation in a compact form.

### *6.1 Linear elastic wave equation*

Introduce a vector $\hat{\mathbf{q}} = (\hat{q}_{ijk})^{\mathrm{T}} = (\hat{q}_{001}, \ldots, \hat{q}_{005}, \hat{q}_{101}, \ldots, \hat{q}_{105}, \ldots, \hat{q}_{NM5})^{\mathrm{T}}$ where the three indices $i, j$ and $k$ represent the $\xi$-coordinate, $\eta$-coordinate and the solution variable, respectively. We define difference operators in terms of Kronecker products that operate on one index at a time.

Let $\mathbf{Q}_\xi = Q_\xi \otimes I_M \otimes I_5$ and $\mathbf{Q}_\eta = I_N \otimes Q_\eta \otimes I_5$ where $Q_\xi$ and $Q_\eta$ are 1D difference operators in the $\xi$- and $\eta$-directions, respectively, satisfying the SBP property (11). The identity operators $I_N$ and $I_M$ are unit matrices of size $(N+1) \times (N+1)$ and $(M+1) \times (M+1)$, respectively. The computation of the spatial differences of $\hat{\mathbf{q}}$ can then be seen as operating on $\hat{\mathbf{q}}$ with one of the Kronecker products, i.e., $\mathbf{Q}_\eta \hat{\mathbf{q}}$ operates on the second index and yields a vector of the same size as $\hat{\mathbf{q}}$ representing the first derivative approximation in the $\eta$-direction. To express the semi-discrete linear elastic wave equation, we also need to define $\hat{\mathbf{A}} = I_N \otimes I_M \otimes \hat{A}$ and $\hat{\mathbf{B}} = I_N \otimes I_M \otimes \hat{B}$. Note that these products are never actually explicitly formed as they are merely theoretical constructs to make the notation more compact. The products correspond well to the actual finite difference implementation, i.e., the approximations of the first derivatives are calculated by operating on successive lines of values in the computational domain. Using the Kronecker products defined earlier, the semi-discrete linear elastic wave equation with constant coefficients including the SAT expression can be written as

$$\frac{d\hat{\mathbf{q}}}{dt} = \mathbf{Q}_\xi(\hat{\mathbf{A}}\hat{\mathbf{q}}) + \mathbf{Q}_\eta(\hat{\mathbf{B}}\hat{\mathbf{q}}) + \widehat{\mathbf{SAT}} \tag{28}$$

where $\widehat{\mathbf{SAT}}$ is the SAT expression in transformed coordinates defined in Equation (25).

### *6.2 Navier–Stokes equations*

For the fluid equations, we employ a similar procedure, i.e., we define vectors for the solution variables $\widehat{\mathbf{U}}' = (\widehat{U}'_{ijk})^{\mathrm{T}} = (\widehat{U}'_{001}, \ldots, \widehat{U}'_{004}, \widehat{U}'_{101}, \ldots, \widehat{U}'_{104}, \ldots, \widehat{U}'_{NM4})^{\mathrm{T}}$, and similarly for the two flux vectors $\widehat{\mathbf{F}}'$ and $\widehat{\mathbf{G}}'$, where again the three indices $i, j$ and $k$ represent the $\xi$-coordinate, $\eta$-coordinate and the solution variable,

respectively. The same difference operators are used as for the linear elastic wave equation. The discretised fluid equation can thus be written as

$$\frac{d\hat{\mathbf{U}}'}{d\tau} = -\mathbf{Q}_\xi \hat{\mathbf{F}}' - \mathbf{Q}_\eta \hat{\mathbf{G}}'. \tag{29}$$

### 6.3 Time integration

The systems (28) and (29) of ordinary differential equations can readily be solved by the classical fourth-order explicit Runge–Kutta method. For the linear elastic wave equation, calling the right-hand side of (28) $\mathbf{f}(t_n, \hat{\mathbf{q}}^n)$ at the time level $n$, we advance the solution to level $n+1$ by performing the stages

$$\begin{aligned}
\mathbf{k}_1 &= \mathbf{f}(t_n, \hat{\mathbf{q}}^n) \\
\mathbf{k}_2 &= \mathbf{f}\left(t_n + \frac{\Delta t}{2}, \hat{\mathbf{q}}^n + \frac{\Delta t}{2}\mathbf{k}_1\right) \\
\mathbf{k}_3 &= \mathbf{f}\left(t_n + \frac{\Delta t}{2}, \hat{\mathbf{q}}^n + \frac{\Delta t}{2}\mathbf{k}_2\right) \\
\mathbf{k}_4 &= \mathbf{f}(t_n + \Delta t, \hat{\mathbf{q}}^n + \Delta t \mathbf{k}_3) \\
\hat{\mathbf{q}}^{n+1} &= \hat{\mathbf{q}}^n + \frac{\Delta t}{6}(\mathbf{k}_1 + 2\mathbf{k}_2 + 2\mathbf{k}_3 + \mathbf{k}_4)
\end{aligned}$$

and similar expressions for the fluid Equation (29). The boundary conditions are updated only after all four stages for the respective field have been completed. That is to say, the structure solution at level $n+1$ is obtained using only the fluid stress at time level $n$. Likewise, the fluid solution at time level $n+1$ is based only on the position and velocity of the structure at time level $n$.

## 7 Results

### *Verification*

Our fluid solver has previously been verified and tested for numerical simulation of Aeolian tones (Müller, 2008) and qualitatively tested for simulation of human phonation on fixed grids (Larsson and Müller, 2009a) as well as moving grids in ALE formulation (Larsson, 2007).

The solver for the linear elastic equations with the SAT expression has been tested with a manufactured solution (Larsson and Müller, 2011) and an academic 2D test case where we obtained a rate of convergence of 3.5–4 in the 2-norm (to be published).

### 7.1 Problem parameters

The initial geometry for the vocal folds is here based on the geometry used in Zhao et al. (2002) for an oscillating glottis with a given time dependence. The geometry chosen by Zhao et al. (2002) is an idealised vocal tract with a time-varying geometry, where the false vocal folds are not taken into account. The initial shape of the vocal tract including the vocal fold is given as

$$r_w(x) = \frac{D_0 - D_{\min}}{4} \tanh s + \frac{D_0 + D_{\min}}{4}, \tag{30}$$

where $r_w$ is the half height of the vocal tract, $D_0 = 5D_g$ is the height of the channel, $D_g = 4\,\mathrm{mm}$ is the average glottis height, $D_{\min} = 1.6\,\mathrm{mm}$ is the minimum glottis height, $s = b|x|/D_g - bD_g/|x|$, $c = 0.42$ and $b = 1.4$. For $-2D_g \le x \le 2D_g$, the function (30) describes the curved parts of the reference configuration for the top and bottom (with a minus sign) vocal folds. The $x$-coordinates for the in- and outflow boundaries are $-4D_g$ and $10D_g$, respectively.

### 7.2 Vocal fold material parameters

The density in the reference configuration is $\rho_0 = 1043\,\mathrm{kg/m^3}$, corresponding to the measured density of vocal fold tissue as reported by Hunter et al. (2004). The Poisson ratio is chosen as $\nu = 0.47$ for the tissue, corresponding to a nearly incompressible material with $\nu = 0.5$ being the theoretical incompressible limit. The Lamé parameters are chosen as $\mu = 3.5\,\mathrm{kPa}$ and $\lambda$ given by $\lambda = 2\mu\nu/(1-2\nu)$.

### 7.3 Fluid model

We use a Reynolds number of 3000 based on the average glottis height $D_g = 0.004\,\mathrm{m}$ and an assumed average velocity in the glottis of $U_m = 40\,\mathrm{m/s}$. We employ these particular values to be able to compare with previously published results by Zhao et al. (2002) and Zhang et al. (2002) and by (Larsson, 2007) and Larsson and Müller (2009a). The Prandtl number is set to 1.0, and the Mach number is 0.2 based on the assumed average velocity and the speed of sound. We deliberately use a lower value for the speed of sound $c_0 = 200\,\mathrm{m/s}$ to speed up the computations. We implemented the higher Mach number by using the stagnation density $\rho_0$, the lowered stagnation speed of sound $c_0$ and $\rho_0 c_0^2$ as reference values of the non-dimensional density, velocity and pressure, respectively. The air density is $1.3\,\mathrm{kg/m^3}$, and the atmospheric pressure is $p_{\mathrm{atm}} = 101325\,\mathrm{Pa}$. The equation of state is the perfect gas law, and we assume a Newtonian fluid. At the inlet, we impose a typical lung pressure during phonation with a small asymmetric perturbation by setting the acoustic pressure to $p_{\mathrm{acoustic}} = p - p_{\mathrm{atm}} = (1 + 0.025\sin 2\pi\eta)2736\,\mathrm{Pa}$, where $\eta = 0$ at the lower vertex and $\eta = 1$ at the upper vertex of the inflow boundary. The outlet pressure is set to atmospheric pressure, i.e., $p - p_{\mathrm{atm}} = 0\,\mathrm{Pa}$.

### 7.4 Numerical simulation

Both fluid and structure use the same set of variables for non-dimensionalisation, and the same time step is used for both fields so that the two solutions can exchange information at the same time levels. The structure grid consists of $81 \times 61$ points for each vocal fold, i.e., for the upper and the lower vocal folds, and the fluid grid has $241 \times 61$ points. The time step is determined by the stability condition for the fluid, which is satisfied here by

requiring $CFL \leq 1$. Since the fluid domain changes with time, the CFL condition puts a stricter constraint on the time step when the glottis is nearly closed. The solution is marched in time with given initial and boundary conditions to dimensional time $t = 12\,\mathrm{ms}$ (total number of time steps 277310).

The acoustic pressure is recorded at four points at $x = 8\,D_g$. Points 1–4 are located at $y = -3D_0/10$, $y = -D_0/10$, $y = D_0/10$, and $y = 3D_0/10$, respectively. Figure 6 shows the computed non-dimensional acoustic pressure $p'/(\rho_0 c_0^2)$ at the four points as a function of the non-dimensional time $t^\star = tc_0/D_g$ for a duration of 7ms in physical time. Large acoustic pressures are recorded as the start-up vortex passes the points during the time interval of about $40 \leq t^\star \leq 90$. The modulus of the acoustic pressure decreases as large vortices pass at $t^\star \approx 150$ and $t^\star \approx 240$. Smaller vortices cause smaller variations of the acoustic pressure. Since the acoustic pressure curves recorded at the four points lie almost on top of each other, the acoustic pressure at $x = 8\,D_g$ slightly upstream of the right boundary proves to behave almost one-dimensionally.

**Figure 6** Non-dimensional acoustic pressure $p'/(\rho_0 c_0^2)$ as a function of non-dimensional time $t^\star = tc_0/D_g$ at 4 points located at $x = 8\,D_g$ and $y = -3D_0/10$, $y = -D_0/10$, $y = D_0/10$, and $y = 3D_0/10$, respectively

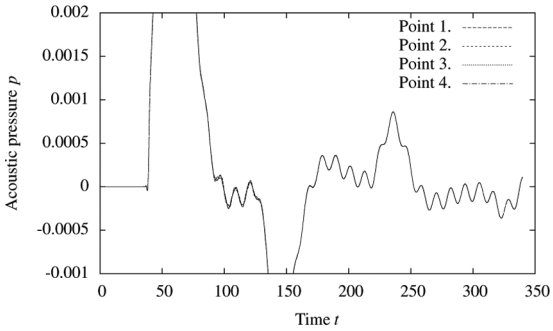


The solution is first integrated to time $t = 6\,\mathrm{ms}$ so that the effect of initial conditions will be negligible. After that, the solution is recorded at consecutive 2 ms intervals as shown in Figure 7 where the vorticity and pressure contours are depicted in the left and right columns, respectively.

Initially, a starting jet is formed in the glottis, which becomes unstable near the exit and creates the beginnings of vortical structures at time $t = 6\,\mathrm{ms}$. Since the boundary conditions are not symmetric with respect to the streamwise centreline, also the solution is not symmetric. In the following, vortices are shed near the glottis and propagate downstream driven by the pressure gradient. The pressure plots indicate a sharp pressure drop just upstream of the orifice. Downstream, the pressure minima occur in the vortex centres as expected.

The observed frequency of the vortex shedding is about 80 Hz, which is comparable to the typical phonation frequencies of 100 Hz for men and 200 Hz for women.

**Figure 7** Vorticity and pressure contours at 2 ms intervals. The left column shows vorticity contours, the right column shows pressure contours. The top row shows the solution evaluated at $t = 6\,\mathrm{ms}$, the second row is at $t = 8\,\mathrm{ms}$ and so on up to $t = 14\,\mathrm{ms}$ (last row). The colorbar in the vorticity column stretches from 0 to $50\,000\,\mathrm{s}^{-1}$ and the contour levels are spaced $3\,750\,\mathrm{s}^{-1}$ apart. For the pressure column, the inflow is at $p = p_\infty + \Delta p$, the outflow is at (approximately) $p = p_\infty$ and the contour levels are spaced 71 Pa apart (see online version for colours)

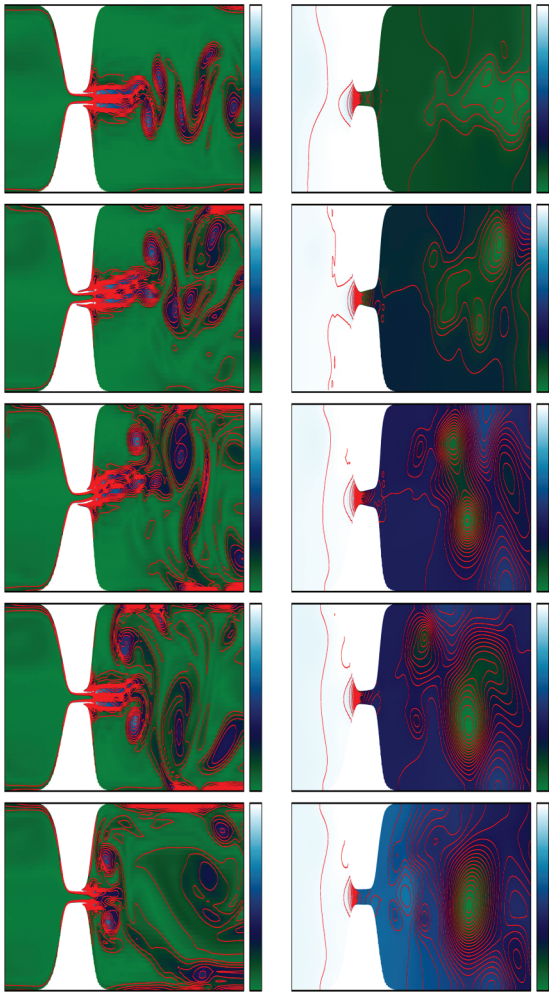

## 8 Conclusions

Our 2D model for the vocal folds based on the linear elastic wave equation in the first-order form and the airflow based on the compressible Navier–Stokes equations in the vocal tract proves to be able to capture the self-sustained pressure-driven oscillations and vortex generation in the glottis. The high-order method for the linear elastic wave equation with a SAT formulation for the boundary conditions ensures a time-stable solution. The fluid and structure fields are simultaneously integrated explicitly in time and boundary data is exchanged only at the end of a time step. With this formulation, there is no need for iterations to find the equilibrium displacement for the structure

depending on the fluid stresses. For the problem we consider here, the limiting factor on the time step is the CFL condition from the compressible Navier–Stokes equations. Since the fluid grid of the vocal tract has more grid points than the structure grids of the vocal folds and the non-linear flow equations are more involved than the linear structure equations, the effort of integrating the linear elastic wave equation to get the structure displacement is small compared with the flow solution.

## Acknowledgements

The current research was funded by the Swedish Research Council under the project 'Numerical Simulation of Respiratory Flow'.

This is a modified version of our paper with the same title presented at the 8th International Conference on CFD in the Oil and Gas, Metallurgical and Process Industries (Skjetne and Olsen, 2011). More details on the assumptions of our 2D model are added in Section 1 Introduction, and Figure 6 is added and discussed in Section 7.4 Numerical simulation.

## References

Carpenter, M.H., Gottlieb, D. and Abarbanel, S. (1994) 'Time-stable boundary conditions for finite-difference schemes solving hyperbolic systems: methodology and application to high-order compact schemes', *J. Comput. Phys.*, Vol. 111, pp.220–236.

Fornberg, B. (1998) *A Practical Guide to Pseudospectral Methods*, Cambridge University Press, Cambridge.

Gustafsson, B. (2008) *High Order Difference Methods for Time-Dependent PDE*, Springer-Verlag, Berlin.

Gustafsson, B., Kreiss, H-O. and Oliger, J. (1995) *Time Dependent Problems and Difference Methods*, John Wiley & Sons, New York.

Hunter, E.J., Titze, I.R. and Alipour, F. (2004) 'A three-dimensional model of vocal fold abduction/adduction', *J. Acoust. Soc. Am.*, Vol. 115, No. 4, pp.1747–1759.

Larsson, M. (2007) *Numerical Simulation of Human Phonation*, Master Thesis, Department of Information Technology, Uppsala University, Sweden.

Larsson, M. (2010) *Numerical Modeling of Fluid-Structure Interaction in the Human Larynx*, PhD Thesis, Norwegian University of Science and Technology, Trondheim, Norway.

Larsson, M. and Müller, B. (2009a) 'Numerical simulation of confined pulsating jets in human phonation', *Computers & Fluids*, Vol. 38, No. 7, pp.1375–1383.

Larsson, M. and Müller, B. (2009b) 'Numerical simulation of fluid-structure interaction in human phonation', in Skallerud, B. and Andersson, H.I. (Eds.): *MekIT 09 Fifth National Conference on Computational Mechanics*, Tapir Academic Press, Trondheim, Norway, pp.261–280.

Larsson, M. and Müller, B. (2010a) 'High order numerical simulation of fluid-structure interaction in human phonation', *Proceedings of ECCOMAS CFD 2010 conference*, 14–17 June, Lisbon, Portugal.

Larsson, M. and Müller, B. (2010b) 'Numerical simulation of fluid-structure interaction in human phonation: Application', in Kreiss, G., Lötstedt, P., Målqvist, A. and Neytcheva, M. (Eds.): *Numerical Mathematics and Advanced Applications 2009* (*Proceedings of ENUMATH 2009 Eighth European Conference on Numerical Mathematics and Advanced Applications, 29 June–3 July 2009*), Uppsala, Sweden, Part 2, Springer-Verlag, Berlin, pp.571–578.

Larsson, M. and Müller, B. (2011) 'Numerical simulation of fluid-structure interaction in human phonation: Verification of structure part', in Hesthaven, J.S. and Rønquist, E.M. (Eds.): *Spectral and High Order Methods for Partial Differential Equations* (Selected Papers *from the ICOSAHOM '09 Conference, 22–26 June 2009*, Trondheim, Norway), Springer-Verlag, Berlin, pp.229–236.

LeVeque, R.J. (2002) *Finite Volume Methods for Hyperbolic Problems*, Cambridge University Press, Cambridge.

Link, G., Kaltenbacher, M., Breuer, M. and Döllinger, M. (2009) 'A 2D finite-element scheme for fluid-solid-acoustic interactions and its application to human phonation', *Methods in Applied Mechanics and Engineering*, Vol. 198, pp.3321–3334.

Luo, H., Mittal, R., Zheng, X., Bielamowicz, S.A., Walsh, R.J. and Hahn, J.K. (2008) 'An immersed-boundary method for flow – structure interaction in biological systems with application to phonation', *J. Comput. Phys.*, Vol. 227, pp.9303–9332.

Müller, B. (1996) *Computation of Compressible Low Mach Number Flow*, Habilitation thesis, ETH Zurich, Zurich, Switzerland.

Müller, B. (2008) 'High order numerical simulation of Aeolian tones', *Computers & Fluids*, Vol. 37, No. 4, pp.450–462.

Poinsot, T.J. and Lele, S.K. (1992) 'Boundary conditions for direct simulations of compressible viscous flows', *J. Comput. Phys.*, Vol. 101, pp.104–129.

Sesterhenn, J., Müller, B. and Thomann, H. (1999) 'On the cancellation problem in calculating compressible low mach number flows' *J. Comput. Phys.*, Vol. 151, pp.597–615.

Strand, B. (1994) 'Summation by parts for finite difference approximations for d/dx', *J. Comput. Phys.*, Vol. 110, pp.47–67.

Titze, I.R. (2000) *Principles of Voice Production*, National Center for Voice and Speech, Iowa City, USA.

Titze, I.R. (2008) 'The human instrument', *Scientific American*, Vol. 298, pp.94–101.

Visbal, M.R. and Gaitonde, D.V. (2002) 'On the use of higher-order finite-difference schemes on curvilinear and deforming meshes', *J. Comput. Phys.*, Vol. 181, pp.155–185.

Zhang, C., Zhao, W., Frankel, S.H. and Mongeau, L. (2002) 'Computational aeroacoustics of phonation, part II', *J. Acoust. Soc. Am.*, Vol. 112, No. 5, pp.2147–2154.

Zhao, W., Frankel, S.H. and Mongeau, L. (2002) 'Computational aeroacoustics of phonation, part I', *J. Acoust. Soc. Am.*, Vol. 112, No. 5, pp.2134–2146.

## Appendix A

The eigenvector matrix $T(k_x, k_y)$ of $P(k_x, k_y)$ reads

$$T(k_x,k_y) = \begin{bmatrix} k_x\tilde{c}_p/\lambda & -k_y & 0 & -k_y & -k_x\tilde{c}_p/\lambda \\ k_y\tilde{c}_p/\lambda & k_x & 0 & k_x & -k_y\tilde{c}_p/\lambda \\ k_x^2\alpha + k_y^2 & -\frac{2k_xk_y\tilde{c}_s\rho}{r^2} & k_y^2 & \frac{2k_xk_y\tilde{c}_s\rho}{r^2} & k_x^2\alpha + k_y^2 \\ 2k_xk_y\mu/\lambda & \rho\tilde{c}_s\bar{k} & -k_xk_y & -\rho\tilde{c}_s\bar{k} & 2\mu k_xk_y/\lambda \\ k_y^2\alpha + k_x^2 & \frac{2k_xk_y\tilde{c}_s\rho}{r^2} & k_x^2 & -\frac{2k_xk_y\tilde{c}_s\rho}{r^2} & k_y^2\alpha + k_x^2 \end{bmatrix} \tag{31}$$

The inverse of this matrix reads

$$T(k_x,k_y)^{-1} = \frac{1}{2r^2}\begin{bmatrix} \frac{k_x\lambda}{\tilde{c}_p} & \frac{k_y\lambda}{\tilde{c}_p} & \frac{k_x^2}{\alpha r^2} & 2\frac{k_yk_x}{\alpha r^2} & \frac{k_y^2}{\alpha r^2} \\ -k_y & k_x & -\frac{k_xk_y}{\rho\tilde{c}_s} & \frac{\bar{k}r^2}{\rho\tilde{c}_s} & \frac{k_xk_y}{\rho\tilde{c}_s} \\ 0 & 0 & -\frac{2\bar{k}}{\alpha} + \frac{4k_y^2}{\beta r^2} & -8\frac{k_xk_y(\lambda+\mu)}{r^2(\lambda+2\mu)} & \frac{2\bar{k}}{\alpha} + 4\frac{k_x^2}{\beta r^2} \\ -k_y & k_x & \frac{k_xk_y}{\rho\tilde{c}_s} & -\frac{\bar{k}r^2}{\rho\tilde{c}_s} & -\frac{k_xk_y}{\rho\tilde{c}_s} \\ -\frac{\lambda k_x}{\tilde{c}_p} & -\frac{\lambda k_y}{\tilde{c}_p} & \frac{k_x^2}{\alpha r^2} & 2\frac{k_yk_x}{\alpha r^2} & \frac{k_y^2}{\alpha r^2} \end{bmatrix} \tag{32}$$

where the parameters are defined by $\bar{k} = (k_x^2 - k_y^2)/(k_x^2 + k_y^2)$, $r = (k_x^2 + k_y^2)^{1/2}$, $\tilde{c}_p = rc_p$, $\tilde{c}_s = rc_s$, $\alpha = (\lambda + 2\mu)/\lambda$ and $\beta = \alpha\lambda/\mu$.

## Nomenclature

| | |
|---|---|
| *Greek symbols* | |
| $\Lambda$ | Eigenvalue matrix for linear elastic equations |
| $\lambda$, $\mu$ | Lamé parameters; $\lambda$ also refers to an eigenvalue |
| $\sigma$ | Cauchy stress tensor |
| $\xi, \eta$ | Computational coordinates |
| *Latin symbols* | |
| $A$, $B$ | Coefficient matrices for the linear elastic wave equation |
| $c_p$, $c_s$ | Primary and secondary wave speeds in the structure |
| $F, G$ | Flux vectors in $x$- and $y$-directions |
| $f, g, h$ | Components of the Cauchy stress tensor $\sigma$ in the structure |
| $F^{c,v}, G^{c,v}$ | Inviscid ($c$) and viscous ($v$) flux vectors |
| $g^{\mathrm{I,II}}$ | Functions representing the boundary conditions for characteristic variables $u^{\mathrm{I,II}}$ |
| $H$ | Diagonal norm matrix associated with $Q$ |
| $J^{-1}$ | Jacobian determinant of coordinate transformation |
| $k = \xi, \eta$ | Computational coordinate |
| $p$ | Pressure in the fluid |
| $Q$ | Finite difference operator |
| $q, \hat{q}$ | Vector of unknowns in the structure in physical and computational coordinates |
| $\hat{\mathbf{q}}$ | Grid function of unknowns in the structure in computational coordinates |
| $R, L$ | Matrices for right and left going characteristic variables at right and left boundaries |
| $\mathrm{SAT}_i^{(k)}$ | Vector value of SAT expression in characteristic variables at grid point $i$ in direction $k = \xi, \eta$ |
| $\overline{\mathrm{SAT}}_i^{(k)}$ | Vector value of SAT expression in standard variables at grid point $i$ in direction $k = \xi, \eta$ |
| $\widehat{\overline{\mathrm{SAT}}}_{i,j}$ | Vector value of total SAT expression in standard variables at grid point $i, j$ |
| $T$ | Matrix of eigenvectors |
| $\bar{\mathbf{t}}$ | Traction from the fluid at fluid-structure interface |
| $t$ | Time |
| $U, \hat{U}$ | Vector of conservative variables in the fluid in physical and computational coordinates |
| $u, v$ | Velocity components in the structure |
| $u^{\mathrm{I,II}}, \mathbf{u}^{\mathrm{I,II}}$ | Characteristic variables corresponding to positive and negative eigenvalues and their corresponding grid functions |
| $\bar{u}(k = k_0, t)$, $\bar{v}(k = k_0, t)$ | Specified boundary conditions on variables $u$, $v$ at $k = k_0$ |
| $\hat{\mathbf{U}}'$ | Grid function of conservative perturbation variables in the fluid in computational coordinates |
| $\mathbf{u}$ | Discrete solution |
| $x, y$ | Cartesian coordinates |
| *Sub/superscripts* | |
| $'$ | Perturbation variables |
| $i, j$ | Indices $i, j$ |
| $n$ | Time level $n$ |